

NMR properties of a one-dimensional Cu-O model

T. Becker, M. Gabay, and T. Giamarchi

Laboratoire de Physique des Solides, CNRS UMR 85002, Université Paris-Sud, 91405 Orsay, France

(July 17, 2000)

We obtain the Knight shifts and the relaxation rates related to the Fermi contact interaction term for a one-dimensional Cu-O model using bosonization technique. We consider the small interaction limit at half-filling and away from half-filling. In this framework we predict that the antiferromagnetic contribution to the relaxation rate of the nuclear oxygen spin is completely suppressed even away from half-filling, when the temperature is low enough. In the strong interaction limit at half-filling we compute the effective Fermi contact interaction performing a Gutzwiller projection. Both limits suggest that the one-dimensional versions of the Mila-Rice and of the Shastry scenarios of transferred hyperfine couplings which were proposed to explain the NMR measurements for High- T_c cuprates fail in a one-dimensional situation.

74.72-h, 76.20.+q, 76.60-k

I. INTRODUCTION

One of the challenging characteristics of the cuprate materials is the importance of magnetic fluctuations and their effect on normal state transport and on superconductivity. This feature is naturally present in theoretical approaches emphasizing strong interactions in 2D. The role of magnetism can also be assessed in other scenarios promoting marginal or nearly antiferromagnetic Fermi liquid (NAFL) behavior. The NAFL framework has been used by Millis, Monien, and Pines¹ to discuss NMR experiments: on the basis of the Mila-Rice² and Shastry³ local terms describing spin fluctuations induced by the hyperfine interactions, these authors were able to compute various Knight shifts and nuclear relaxation times. However, there are critical remarks and further details to this theory,⁴⁻⁷ and also other theories introduced in order to interpret the behavior of the various Knight shifts and nuclear relaxation times in high- T_c superconductors, which we do not discuss here.⁸

In this paper, we will follow the basic assumption of Mila and Rice that it is necessary to include a sizeable isotropic hyperfine interaction term to fit the data of NMR experiments in High- T_c cuprates. Thus in the following we will focus our interest on this contribution which comes mainly from the Fermi contact interaction between a nucleus and its surrounding partially filled s orbitals, namely the 4s orbital for copper and the 3s orbital for oxygen. Experiments have shown that the magnetic properties are described by a single-spin component model. In the weak interaction limit, this single-spin degree of freedom could be associated with the strongly hybridized Cu-3d—O-2p anti-bonding band,^{6,7} whereas in the strong interaction limit it is associated with the nearly localized Cu-3d spin.^{2,3,7} Within the local picture, the contrasting NMR behavior seen on the Cu and O sites arises from their different hyperfine form factors. These are nothing but the Fourier transforms of the Fermi contact interaction terms approximated by a sum over surrounding localized next-neighbor Cu-3d spins.

One of the (many) complications concerning the

physics of cuprate materials is that there is still no consensus about what should be the correct theoretical approach to treat correlations in 2D: Is the ground state Fermi liquid or non-Fermi liquid like? Can one treat interactions perturbatively, or is it more appropriate to treat kinetic terms as corrections in the strongly interacting limit? In the latter category, working out a consistent treatment of the non-double occupancy constraint is still an open issue.

By contrast, one-dimensional systems offer a perfect testing ground for the study of magnetic fluctuations. Since in one dimension it is possible to treat correlation effects properly both in the limit of weak and strong interactions, such models allow to compute explicitly the dependence of the relaxation. This allows to get some feeling for the effects of doping. In addition to the insight that such study allows to gain for higher dimensional models, there are explicit realizations of one-dimensional systems, such as the Bechgaard salts or copper germanate compounds.^{9,10}

For these reasons, we choose to investigate hyperfine interactions in the one-dimensional version of the Cu-O model. This allows us to extract form factors both in the insulating and in the doped regime, without assuming a specific form of the Fermi contact interaction term. We can then compare the exact results with the predictions that the standard approximation schemes used in two dimensions would give in the one-dimensional situation.

The paper is organized as follows. In section II, we introduce the model in one dimension, as well as the three different approximations used to describe the magnetic relaxation processes related to the Fermi contact interaction term, namely that due to Mila-Rice,² to Shastry,³ and to Bulut.⁷ In section III, we solve the full model for weak interactions as compared to the bandwidth. We obtain spin-spin correlation functions and discuss the Knight shift K and the relaxation rate $1/T_1$ in detail. We compare our results with the prediction of the Bulut model, which is applicable for weak interactions. Section IV solves the problem in the opposite limit of very strong interactions using a Gutzwiller projection elimi-

nating double occupation on the copper sites. We again compare our results with the one-dimensional extrapolation of the Mila-Rice and of the Shastry approximations. A general discussion of our results is presented in section V. Since NMR data on organic¹¹ and inorganic quasi-1D compounds seem to give an essentially isotropic relaxation rate, the body of the paper mostly focuses on the isotropic contribution to the hyperfine interaction. Yet, for the sake of completeness and in view of the fact that K can be anisotropic (see below in section V) we discuss the effect of anisotropic hyperfine terms in Appendix A: these terms only modify prefactors in the expressions of $1/T_1$ and of K . Appendix B and C offer details of our calculations.

II. DEFINITION OF THE MODELS

A. The four-band model

We consider a system with two different atoms per unit cell (Cu and O). In order to describe the ground state properties, we take into account the 3d and 2p orbitals on Cu and O respectively. The related hole states are represented in Fig. 1 and denoted by a and b in the following. Since the coupling to the nuclear spin via the Fermi contact interaction occurs only for partially filled s orbitals, we also have to retain the Cu-4s and O-3s shells (denoted by A and B) to correctly obtain the desired NMR properties. The Hamiltonian describing the system can thus be written as

$$H = H_0 + H_S + H_N , \quad (2.1)$$

where H_0 contains the electronically relevant orbitals a and b . H_S describes the coupling of orbitals a and b to orbitals A and B . As indicated in Fig. 1, the orbitals A and B are basically filled and produce only small corrections to the electronic term represented by H_0 , so that we will treat H_S as a perturbation. Finally, H_N describes the coupling of the orbitals A and B to the nuclear spins and will be treated as a small – time dependent – perturbation in linear response.

The main contribution, H_0 , is given by

$$H_0 = H_T + H_U , \quad (2.2)$$

where

$$H_T = \sum_j \epsilon_a n_{aj} + \epsilon_b n_{bj} - \sum_{j\sigma} t_{ab} [a_{j\sigma}^\dagger (b_{j\sigma} + b_{j-1,\sigma}) + \text{h.c.}] \quad (2.3)$$

$$H_U = \sum_j U_a n_{aj\uparrow} n_{aj\downarrow} + \sum_j U_b n_{bj\uparrow} n_{bj\downarrow} . \quad (2.4)$$

Here t_{ab} describes the hopping between the Cu-3d and the O-2p orbitals with the phase conventions shown in

Fig. 2. U_a and U_b are the local repulsions on the copper and oxygen sites as shown in Fig. 1. The Coulomb repulsions U_A and U_B can be ignored assuming that energy cost considerations discourage processes in which two holes are excited in one s orbital. A nearest neighbor interaction U_{ab} could also be added to the model to generate a phase transition to a superconducting phase,¹² but here our study deals with the vicinity of the half-filled case, i.e. near the antiferromagnetic phase, and we will ignore U_{ab} .

The coupling between the orbitals a, b and A, B reads

$$H_S = \sum_j \epsilon_A n_{Aj} + \epsilon_B n_{Bj} + \sum_{j\sigma} t_{Ba} [B_{j\sigma}^\dagger (a_{j+1,\sigma} - a_{j\sigma}) + \text{h.c.}] + \sum_{j\sigma} t_{Ab} [A_{j\sigma}^\dagger (b_{j\sigma} + b_{j-1,\sigma}) + \text{h.c.}] + \sum_{j\sigma} t_{Aa} [A_{j\sigma}^\dagger (a_{j+1,\sigma} + a_{j-1,\sigma}) + \text{h.c.}] \quad (2.5)$$

with the phase conventions of Fig. 2. The density operators $n_{\eta j}$ in (2.3), (2.4), and (2.5) are the standard ones

$$n_{\eta j} = \sum_\sigma n_{\eta j\sigma} = \sum_\sigma \eta_{j\sigma}^\dagger \eta_{j\sigma} , \quad (2.6)$$

where $\eta = a, b, A, B$.

Finally, the isotropic coupling to the nuclear spins (**I** for the copper atom and **J** for the oxygen atom) is given by

$$H_N = \sum_j C_A \mathbf{I}_j \mathbf{S}_{Aj} + C_B \mathbf{J}_j \mathbf{S}_{Bj} , \quad (2.7)$$

where similarly to (2.6) the spin operators are given by

$$\mathbf{S}_{\eta j} = \frac{1}{2} \sum_{\sigma_1 \sigma_2} \eta_{j\sigma_1}^\dagger \boldsymbol{\sigma}_{\sigma_1 \sigma_2} \eta_{j\sigma_2} . \quad (2.8)$$

The coupling constant for the electron-nuclear interaction is given by $C_\eta = (8\pi/3)|\psi_\eta(0)|^2 \gamma_n g \mu_B \hbar$, which is proportional to the local hole density for the respective s orbitals at the origin. $\sigma_{\sigma_1 \sigma_2}$ are the Pauli matrices.

B. Reduced models

In 1D, the Hamiltonian (2.1) can explicitly be expressed in terms of bose fields. This allows for a full treatment, in which H_0 , H_S , and H_N are all treated on an equal footing. This is the route we follow in section III. In higher dimension there is still no solution of the fully interacting problem. So various approximation schemes have been devised and applied to each of the pieces of H separately. These lead to effective "nuclear" Hamiltonians : the Mila-Rice and the Shastry model for strong

interactions and the Bulut model for weak interactions. Typically, the analysis by Mila-Rice and Shastry starts from a partially projected Hamiltonian

$$H = \hat{P}H_0\hat{P} + H_S + H_N . \quad (2.9)$$

The first part gives the t-J model or at half-filling the Heisenberg model, which contains the dynamics related to the Cu-3d and O-2p orbitals. The second part contains the unprojected degrees of freedom related to the Cu-4s and O-3s orbitals, as well as the electron-nuclear interaction part. Further approximations for H_S and H_N lead to the Mila-Rice model or to the Shastry model (see below). In the weak interaction limit, Bulut et al. have proposed an RPA treatment of H_0 in combination with the effective electron-nuclear interaction term of Mila-Rice and Shastry.

Before we turn to the full solution of the model, let us review the main features of such approximations when applied to our one-dimensional system. This will allow us to contrast the predictions of the 1D version of these three models and the results obtained for the four-band model, which may provide some clue to the validity of these approaches for strongly correlated systems.

1. The Mila-Rice model for strong interaction

The model defined in (2.1) is approximated by

$$H \simeq H_0^{Mi} + H_N^{Mi} . \quad (2.10)$$

H_0^{Mi} is the approximation for (2.2) and denotes, at half-filling, a Heisenberg model for local Cu-3d spins generated by

$$H_0^{Mi} = \hat{P}[H_0(U_b = 0)]\hat{P} , \quad (2.11)$$

where \hat{P} is the Gutzwiller projection operator which prohibits doubly occupied Cu-3d states. The additional unprojected part (2.5) with $t_{Aa} = t_{Ba} = 0$ and the electron-nuclear interaction part (2.7) are approximated by

$$H_N^{Mi} = \sum_j C_A \mathbf{I}_j \mathbf{S}_{Aj}^{Mi} , \quad (2.12)$$

where

$$\mathbf{S}_{Aj}^{Mi} = F_{Aa}^{Mi} (\mathbf{S}_{a,j-1} + \mathbf{S}_{a,j+1}) . \quad (2.13)$$

Thus \mathbf{S}_{Aj}^{Mi} is the Mila-Rice approximation for the original spin \mathbf{S}_{Aj} used to explain the NMR experiments measured on the copper sites. $F_{Aa}^{Mi} = |\lambda_{Aa}^{Mi}|^2$ denotes the effective overlap between one Cu-4s spin with a neighboring Cu-3d spin. In the Mila-Rice model only hopping processes via the O-2p orbitals are included, whereas the direct hopping between Cu-3d and Cu-4s orbitals is ignored. In Ref. 2 Mila and Rice perform a quantum chemical

analysis without including interaction effects, so we will do the same and propose for the amplitudes

$$\lambda_{Aa}^{Mi} = -\frac{t_{Aa}t_{ab}}{(\epsilon_a - \epsilon_A)(\epsilon_a - \epsilon_b)} . \quad (2.14)$$

This result is obtained by a projection in real space of a Cu-4s orbital onto a neighboring Cu-3d orbital for $U_a = 0$. The Fourier transform of (2.13) is given by

$$\mathbf{S}_{Ap}^{Mi} = F_{Aa}^{Mi}(p) \mathbf{S}_{ap} \quad (2.15)$$

with the Mila-Rice form factor

$$F_{Aa}^{Mi}(p) = 2F_{Aa}^{Mi} \cos(pa) . \quad (2.16)$$

2. The Shastry model for strong interaction

The approximation proposed by Shastry in Ref. 3 is given by

$$H \simeq H_0^{Sh} + H_N^{Sh} , \quad (2.17)$$

where

$$H_0^{Sh} = \hat{P}[H_0(U_b = 0, U_a = \infty)]\hat{P} \quad (2.18)$$

leads to the Heisenberg model at half-filling and to the t-J model for a doped system with strong repulsion on the copper sites. The electron-nuclear interaction part reads

$$H_N^{Sh} = \sum_j C_A \mathbf{I}_j \mathbf{S}_{Aj}^{Sh} + C_B \mathbf{J}_j \mathbf{S}_{Bj}^{Sh} , \quad (2.19)$$

where the spins $\mathbf{S}_{\eta j}^{Sh}$ are approximated by a linear combination of unprojected Cu-3d orbitals

$$\begin{aligned} \mathbf{S}_{Aj}^{Sh} &= F_{Aa}^{Sh} (\mathbf{S}_{a,j-1} + \mathbf{S}_{a,j+1}) \\ &+ F_{Ab}^{Sh} (\mathbf{S}_{bj} + \mathbf{S}_{b,j-1}) \\ &\cong F_{Aa}^{Sh} (\mathbf{S}_{a,j-1} + \mathbf{S}_{a,j+1}) \end{aligned} \quad (2.20)$$

and

$$\mathbf{S}_{Bj}^{Sh} = F_{Ba}^{Sh} (\mathbf{S}_{aj} + \mathbf{S}_{a,j+1}) \quad (2.21)$$

with the coefficients

$$F_{Aa}^{Sh} = |\lambda_{Aa}^{Sh}|^2 = \left(\frac{t_{Aa}}{\epsilon_A - \epsilon_a} \right)^2 \quad (2.22)$$

$$F_{Ab}^{Sh} = |\lambda_{Ab}^{Sh}|^2 = \left(\frac{t_{Ab}}{\epsilon_A - \epsilon_b} \right)^2 \quad (2.23)$$

$$F_{Ba}^{Sh} = |\lambda_{Ba}^{Sh}|^2 = \left(\frac{t_{Ba}}{\epsilon_B - \epsilon_a} \right)^2 . \quad (2.24)$$

For finite doping, it is assumed in Ref. 3 that the spin degrees of freedom related to \mathbf{S}_{bj} are quenched in a Zhang-Rice singlet.¹³ This assumption justifies the second approximation done in (2.20). Further, Shastry includes

only the direct couplings (2.22) up to second order proportional to t_{Aa}^2 for the relaxation of the nuclear copper spin and ignores the fourth order contributions proportional to $t_{ab}^2 t_{Ab}^2$ via the O-2p orbital as proposed by Mila and Rice. The Fourier transform of the approximated spins $\mathbf{S}_{\eta j}^{Sh}$ reads

$$\mathbf{S}_{\eta p}^{Sh} = 2F_{\eta a}^{Sh}(p)\mathbf{S}_{ap} \quad (2.25)$$

with

$$F_{Aa}^{Sh}(p) = 2F_{Aa}^{Sh} \cos(pa) \quad (2.26)$$

$$F_{Ba}^{Sh}(p) = 2F_{Ba}^{Sh} \cos(pa/2). \quad (2.27)$$

For the uniform contribution ($p \sim 0$) all form factors are finite, but for the antiferromagnetic wave vector ($p \sim \pi/a$) the form factor vanishes for the oxygen sites, whereas it stays finite for the copper sites. Thus (2.16), (2.26), and (2.27) are the one-dimensional analogs of the NMR Mila-Rice and Shastry form factors for High-T_c cuprates.

3. The Bulut model for weak interaction

In Ref. 7, Bulut et al. used a weak interaction RPA calculation combined with an electron-nuclear interaction as proposed by Mila-Rice and Shastry to compute NMR related quantities for the High-T_c cuprates. The one-dimensional analog reads

$$H \simeq H_0^{Bu} + H_N^{Bu}. \quad (2.28)$$

In two dimensions, H_0^{Bu} is obtained by applying the RPA method to the 2D version of (2.2) with $U_b = 0$. In one dimension, we can treat all the interaction terms (U_a, U_b) of the original Hamiltonian H_0 by means of bosonization and of renormalization-group theory. Finally, the electron-nuclear interaction term H_N^{Bu} is given in analogy to (2.19) replacing the approximated spins by

$$\mathbf{S}_{Aj}^{Bu} = F_{Aa}^{Bu} (\mathbf{S}_{a,j-1} + \mathbf{S}_{a,j+1}) \quad (2.29)$$

$$\mathbf{S}_{Bj}^{Bu} = F_{Ba}^{Bu} (\mathbf{S}_{aj} + \mathbf{S}_{a,j+1}). \quad (2.30)$$

In Ref. 7, the parameters $F_{\eta a}^{Bu}$ are undefined and could in general include all possible overlaps of the Cu-4s and O-3s orbitals with the Cu-3d orbitals in the sense of Mila-Rice and Shastry. The coefficient for the oxygen will be

$$F_{Ba}^{Bu} = |\lambda_{Ba}^{Bu}|^2 = |\lambda_{Ba}^{Sh}|^2, \quad (2.31)$$

and is thus the same as that proposed by Shastry, whereas the coefficient for copper

$$F_{Aa}^{Bu} = |\lambda_{Aa}^{Bu}|^2 = |\lambda_{Aa}^{Sh} + \lambda_{Aa}^{Mi}|^2 \quad (2.32)$$

includes additional combined terms of third order proportional to $t_{Aa} t_{Ab} t_{ab}$, which are absent in the Mila-Rice and the Shastry model. The form factors correspond to

$$F_{Aa}^{Bu}(p) = 2F_{Aa}^{Bu} \cos(pa) \quad (2.33)$$

$$F_{Ba}^{Bu}(p) = 2F_{Ba}^{Bu} \cos(pa/2). \quad (2.34)$$

III. THE WEAK INTERACTION LIMIT

Let us now solve the full model (2.1) when interactions are weak compared to the bandwidth. This allows us to use the bosonization technique for treating interactions in the undoped as well as in the doped case.

A. NMR properties of the four-band model

1. Reduction to an effective single-band Hamiltonian

Instead of working with the basis a, b it is more convenient to diagonalize (2.3) within a unit cell, and to introduce the bonding and anti-bonding bands. Using the transformation

$$\begin{aligned} a_{k\sigma} &= [\cos(\gamma_k)\alpha_{k\sigma} - \sin(\gamma_k)\beta_{k\sigma}] e^{-i\frac{ka}{2}} \\ b_{k\sigma} &= \sin(\gamma_k)\alpha_{k\sigma} + \cos(\gamma_k)\beta_{k\sigma} \end{aligned} \quad (3.1)$$

with

$$\tan(2\gamma_k) = \frac{2t_{ab}}{\epsilon} \cos(ka/2) \quad , \quad \gamma_k \in \left[0, \frac{\pi}{4}\right] \quad (3.2)$$

the kinetic energy (2.3) becomes

$$H_T = \sum_{k\sigma} \left[\epsilon_\alpha(k)\alpha_{k\sigma}^\dagger \alpha_{k\sigma} + \epsilon_\beta(k)\beta_{k\sigma}^\dagger \beta_{k\sigma} \right], \quad (3.3)$$

where the state $|\alpha_{k\sigma}\rangle$ refers to the lower Hubbard band with energy $\epsilon_\alpha(k) = -\epsilon/\cos(2\gamma_k)$, and the state $|\beta_{k\sigma}\rangle$ to the upper one with energy $\epsilon_\beta(k) = \epsilon/\cos(2\gamma_k)$. In the absence of interactions the chemical potential μ lies in the α -band both for the undoped and for the doped system, and one can ignore the β -band, which is at least $\epsilon_b - \epsilon_a = 2\epsilon$ higher in energy. The same property holds when the interaction terms (2.4) are added to (2.3), given that in the weak coupling limit $U_b, U_a \ll 2t_{ab}^2/\epsilon$. Correlation effects in 1D will strongly affect the α -band states, thus in the following we ignore the terms containing β -operators when substituting (3.1) into (2.4).

Substituting (3.1) into (2.5) and performing a first order perturbation theory with respect to H_S , all operators in (2.1) can be written as

$$\eta_{k\sigma} \cong \lambda_{\eta\alpha}(k)\alpha_{k\sigma} \quad (3.4)$$

with

$$\begin{aligned} \lambda_{a\alpha}(k) &= \cos(\gamma_k)e^{-i\frac{ka}{2}} \\ \lambda_{b\alpha}(k) &= \sin(\gamma_k) \\ \lambda_{A\alpha}(k) &= \frac{2t_{Aa} \cos(ka)}{\epsilon_\alpha(k) - \epsilon_A} \cos(\gamma_k)e^{-i\frac{ka}{2}} \\ &+ \frac{2t_{Ab} \cos(ka/2)}{\epsilon_\alpha(k) - \epsilon_A} \sin(\gamma_k)e^{-i\frac{ka}{2}} \\ \lambda_{B\alpha}(k) &= \frac{2it_{Ba} \sin(ka/2)}{\epsilon_\alpha(k) - \epsilon_B} \cos(\gamma_k). \end{aligned} \quad (3.5)$$

Here we have assumed an unperturbed ground state $|\alpha^{(1)}\rangle \cong |\alpha\rangle$. Thus (3.4) implies that (2.1) reduces to an effective single-band Hamiltonian.

2. The Continuum limit

We can now use the standard techniques in order to treat interacting one-dimensional systems. Restricting ourselves to the low energy physics regime we make the usual approximation valid for 1D systems, i.e. we linearize the spectrum close to the Fermi points, as shown in Fig. 3. Then the Hamiltonian (2.2) is reduced to

$$H_T = \sum_{r=\pm, q, \sigma} r v_F q \alpha_{rq\sigma}^\dagger \alpha_{rq\sigma} \quad (3.6)$$

$$H_U = \sum_{\mathbf{r}, \mathbf{q}} \frac{U(\mathbf{r})}{N} \alpha_{r_1, q_1 + q_3 \uparrow}^\dagger \alpha_{r_2, q_2 - q_3 \downarrow}^\dagger \alpha_{r_3, q_2 \downarrow} \alpha_{r_4, q_1 \uparrow}, \quad (3.7)$$

where $\mathbf{r} = (r_1, r_2, r_3, r_4)$ and $\mathbf{q} = (q_1, q_2, q_3)$. $U(\mathbf{r})$ parameterizes the repulsive interaction in the continuum limit and is given in terms of the standard notations as

$$\begin{aligned} U(\pm, \pm, \pm, \pm) &\equiv U_o \\ U(\pm, \mp, \mp, \pm) &\equiv U_o \\ U(\pm, \mp, \pm, \mp) &\equiv U_s \\ U(\pm, \pm, \mp, \mp) &\equiv U_c. \end{aligned} \quad (3.8)$$

U_o refers to the two forward scattering processes, U_s to the backward scattering, and U_c to the umklapp scattering process that occurs at half-filling. The relation to the local repulsions defined in (2.4) is given by

$$\begin{aligned} U_o &= U_{b\alpha} + U_{a\alpha} > 0 \\ U_s &= U_{b\alpha} + U_{a\alpha} > 0 \\ U_c &= U_{b\alpha} - U_{a\alpha} < 0, \end{aligned} \quad (3.9)$$

where $U_{\eta\alpha}$ is the short notation for the projected Coulomb energies $U_\eta |\lambda_{\eta\alpha}(k_F)|^4$.

As usual for interacting one-dimensional systems, it is useful to introduce a boson representation of the fermion operators, related to the charge and spin density fluctuations. Since the technique is standard, we only recall the main steps and refer the reader to the literature.^{14–17} We rewrite the original density operators in terms of a linear combination of charge ($\nu = c$) and spin ($\nu = s$) density operators for each branch

$$\rho_{r\sigma} = (\rho_{rc} + \sigma \rho_{rs})/\sqrt{2}. \quad (3.10)$$

These density operators define the phase fields

$$\begin{aligned} \Phi_\nu(x) &= -\frac{i\pi}{L} \sum_{r, q \neq 0} \frac{1}{q} e^{-a|q|/2 - iqx} \rho_{r\nu} \\ \Theta_\nu(x) &= \frac{i\pi}{L} \sum_{r, q \neq 0} \frac{r}{q} e^{-a|q|/2 - iqx} \rho_{r\nu}. \end{aligned} \quad (3.11)$$

All operators can be expressed in terms of the boson fields (3.11), and the fermion operator reads:

$$\alpha_{r\sigma}(x) = \frac{1}{\sqrt{2\pi a}} e^{irk_F x - \frac{i}{\sqrt{2}} [r(\Phi_c + \sigma \Phi_s) - (\Theta_c + \sigma \Theta_s)]}. \quad (3.12)$$

The complete Hamiltonian becomes

$$H = (H_0^c + H_U^c) + (H_0^s + H_U^s) + H_N, \quad (3.13)$$

where

$$H_0^\nu = \int \frac{dx}{2\pi} \left[(u_\nu K_\nu)(\pi \Pi_\nu)^2 + \left(\frac{u_\nu}{K_\nu} \right) (\partial_x \Phi_\nu)^2 \right] \quad (3.14)$$

is a quadratic part containing only charge or spin degrees of freedom (with $\nu = c, s$). In (3.14), the variable $\Pi_\nu = \partial_x \Theta_\nu$ is the momentum density conjugate to Φ_ν , and thus they respect the commutation relation $[\Phi_\nu(x), \Pi_\nu(x')] = i\delta(x - x')$. The interaction terms are given by

$$\begin{aligned} H_U^c &= \int dx \frac{2aU_{b\alpha}}{(2\pi a)^2} \cos[\sqrt{8}\Phi_c - \delta x] \\ &\quad - \int dx \frac{2aU_{a\alpha}}{(2\pi a)^2} \cos[\sqrt{8}\Phi_c - \delta(x - a/2)] \end{aligned} \quad (3.15)$$

$$H_U^s = \int dx \frac{2aU_s}{(2\pi a)^2} \cos[\sqrt{8}\Phi_s]. \quad (3.16)$$

Here $\delta = 4k_F - 2\pi/a$ is proportional to the doping of the system with respect to the half-filled case shown in Fig. 1 (for which $k_F = \pi/2a$). Using this representation we suppose to work with a fixed number of particles, since k_F is directly related to the filling. Finally, the isotropic electron-nuclear interaction part could be written as

$$H_N = \int dx [C_A \mathbf{I}(x) \mathbf{S}_A(x) + C_B \mathbf{J}(x) \mathbf{S}_B(x)], \quad (3.17)$$

where H_N is the projection of (2.7) onto the α -band using (2.8) and (3.4). The projected spin operators \mathbf{S}_η are expressed in terms of (3.12). For example, the z -component of the spin operator \mathbf{S}_η can be represented as a sum of $p \sim 0$ and $p \sim 2k_F$ components as

$$S_\eta^z(x) = |\lambda_{\eta\alpha}(k_F)|^2 [\bar{s}_\alpha(x) + \tilde{s}_{\eta\alpha}(x)], \quad (3.18)$$

where the non-oscillatory part is given by

$$\bar{s}_\alpha(x) = -\frac{1}{\sqrt{2\pi}} (\partial_x \Phi_\alpha) \quad (3.19)$$

and the oscillatory part by

$$\tilde{s}_{\eta\alpha}(x) = \frac{1}{\pi a} \sin[\sqrt{2}\Phi_\alpha] \sin[2k_F(x - x_\eta) - \sqrt{2}\Phi_\alpha]. \quad (3.20)$$

The difference between the copper and the oxygen sites is reflected in the value of x_η and affects the oscillatory part; indeed, for copper $x_a = x_A = a/2$ and for oxygen

$x_b = x_B = 0$ as a consequence of the different phase factors in (3.5).

In (3.14), the u_ν are the new velocities for the ν -excitation and the K_ν are the Luttinger liquid parameters controlling the anomalous exponents in the correlation functions. For weak coupling, they are related to the interactions in (3.7) by

$$\begin{aligned} u_s K_s &= u_c K_c = v_F \\ u_s / K_s &= v_F - a U_o / \pi \\ u_c / K_c &= v_F + a U_o / \pi. \end{aligned} \quad (3.21)$$

Since the Luttinger liquid representation is more general than the perturbative result for small interactions, it is also applicable when the interactions are strong. The quadratic Hamiltonian can be viewed in this case as an effective Hamiltonian describing the low-energy properties of the system, provided that the correct Luttinger liquid parameters are used. Such a smooth connection between weak and strong coupling has been proven for single-band models,^{18,19} and a similar Luttinger representation has been shown to work for the case of the two-band model.^{12,20} Equations (3.13–3.17) define the four-band model, and the NMR properties can be computed through H_N .

3. Correlation functions at zero temperature

We focus here on the spin-spin correlation functions relevant for NMR and for neutron scattering experiments. The general form of these functions is

$$R_{\eta\eta'}(x, \tau) = \langle T_\tau S_{\eta'}^z(x, \tau) S_\eta^z(0, 0) \rangle - \langle S_{\eta'}^z \rangle \langle S_\eta^z \rangle, \quad (3.22)$$

and it describes correlations between different orbitals η and η' at different points in Euclidean space-time. Here we introduce the decomposition of this function into a non-oscillatory and an oscillatory part

$$R_{\eta\eta'}(x, \tau) = \bar{R}_{\eta\eta'}(x, \tau) + \cos(2k_F x) \tilde{R}_{\eta\eta'}(x, \tau), \quad (3.23)$$

since the behavior of these functions will be very different for one-dimensional systems.

Because of the doping dependence in the cosine terms in (3.15), the behavior of the system will quite clearly be different for zero and for finite doping. At half-filling, one sees from (3.21), (B2), and (B3) that charge excitations are massive (c_m), whereas spin excitations are in the massless regime (s_o). One recovers the standard Mott or charge-transfer insulator with the massless excitations corresponding to a Heisenberg-like exchange. In the doped case, the term (3.15) is irrelevant because of the oscillatory factor δx . However, at short distances or for short times this term is still small, and the cosine term will influence the behavior of the system. We thus distinguish between two different regimes for the doped case: we assume that for intermediate distances

($a \ll x \ll l_\delta$) the system remains in the (c_m, s_o) -phase as mentioned before for the half-filled case, and when distances are larger than l_δ , the system will be in the (c_o, s_o) -phase because the umklapp process becomes ineffective. The characteristic length separating these two regimes denotes essentially the distance between two charge domain walls and is given by $l_\delta = 2\pi/\delta$.

Due to the spin-charge separation in (3.13), each part of the correlation function (3.23) will factorize into independent averages over the spin (s_o) and the charge sector (c_o or c_m), and will only depend on the characteristic distance $r_\nu = [(u_\nu \tau)^2 + x^2]^{1/2}$ between two points in Euclidean space-time (with $\nu = s, c$). Details about the correlation functions in the various regimes (c_i, s_i) are explained in Appendix B. Substituting (3.18–3.20) in (3.22), the non-oscillatory contribution to the correlation function is given by

$$\bar{R}_{\eta\eta'} = |\lambda_{\eta\alpha}|^2 |\lambda_{\eta'\alpha}|^2 \bar{R}_\alpha(r_s), \quad (3.24)$$

where $\bar{R}_\alpha(r_s) = (2\pi r_s)^{-2}$ depends only on the spin degrees of freedom and is thus completely independent of the coexisting charge phase. Notice that this function is also independent of the orbitals η and η' , and thus there is no fundamental difference between copper and oxygen contributions.

For the oscillatory part of the spin-spin correlation functions, the situation will be quite different. We restrict ourselves to the calculation of correlation functions between identical orbitals ($\eta = \eta'$). Using averages over the charge and spin sectors of the Hamiltonian (3.13), these functions can be reexpressed as

$$\tilde{R}_{\eta\eta}^{c_m, s_o} = \frac{|\lambda_{\eta\alpha}|^4}{(2\pi a)^2} \tilde{R}_{\eta\alpha}^{c_m}(r_c) \tilde{R}_\alpha^{s_o}(r_s) \quad (3.25)$$

in the massive charge regime and as

$$\tilde{R}_{\eta\eta}^{c_o, s_o} = \frac{|\lambda_{\eta\alpha}|^4}{(2\pi a)^2} \tilde{R}_\alpha^{c_o}(r_c) \tilde{R}_\alpha^{s_o}(r_s) \quad (3.26)$$

in the massless charge regime. The newly defined correlation functions in the massless phases (ν_o) are given by

$$\tilde{R}_\alpha^{\nu_o}(r_\nu) = (a/r_\nu)^{K_\nu^*} F(r_\nu). \quad (3.27)$$

The function $F(r_\nu)$ describes the corrections to the Luttinger Liquid behavior which come from the flow to the fixed point²¹. To lowest order, $F(r_\nu)$ can be approximated by 1. The renormalized Luttinger liquid parameters K_ν^* for a spin symmetric model with repulsive interaction are restricted to

$$K_s^* = 1 \quad \text{and} \quad 0 \leq K_c^* \leq 1. \quad (3.28)$$

The value of the renormalized Luttinger liquid parameter K_c^* depends on the interactions. For weak interaction, K_c^* is close to 1, and it decreases as interactions become more repulsive.

The correlation functions in (3.25) which are characterized by the massive charge phase are given by

$$\begin{aligned}\tilde{R}_{A\alpha}^{cm}(r_c) &= 2 \cosh[K_c K_0(m_c r_c)](m_c a)^{K_c} \\ \tilde{R}_{B\alpha}^{cm}(r_c) &= 2 \sinh[K_c K_0(m_c r_c)](m_c a)^{K_c}\end{aligned}\quad (3.29)$$

and depend on the chosen orbital η . Thus, the behavior for copper and oxygen will be quite different. It depends on the distance r_c , the mass m_c , and the stiffness constant K_c . In general, for distances larger than $l_{m_c} = 1/m_c$, the function $\tilde{R}_{A\alpha}^{cm}$ for copper tends to a finite constant, whereas $\tilde{R}_{B\alpha}^{cm}$ for oxygen tends exponentially to zero.

4. The asymptotic expressions at finite temperature

In order to obtain the temperature dependent correlation function $\tilde{R}_{\eta\eta}(x, \tau, \beta)$, we will only use the asymptotic expressions of (3.29). We recover a Luttinger liquid behavior, and the temperature dependence can easily be obtained with the help of the conformal symmetry;²² indeed, we only need to replace $r_\nu(x, \tau)$ by $r_\nu(x, \tau, \beta)$ where

$$r_\nu(x, \tau, \beta) = \frac{u_\nu \beta}{\pi} \sqrt{\sinh\left[\frac{x - iu_\nu \tau}{u_\nu \beta/\pi}\right] \sinh\left[\frac{x + iu_\nu \tau}{u_\nu \beta/\pi}\right]}. \quad (3.30)$$

The relevant asymptotic expressions at half-filling and away from half-filling depend on the relative magnitudes of the various characteristic lengths of the system, namely the lengths related to the mass, l_{m_c} , and to the doping, l_δ , as well as the thermal length $l_\beta = \min\{(u_c \beta)^{-1}, (u_s \beta)^{-1}\}$. For half-filling ($\gamma = 0$) at low temperature, we are in the regime where $l_\beta \gg r_c \gg l_{m_c}$ and $l_\delta = \infty$, thus we can approximate the oscillatory charge contribution in (3.25), and the functions are simplified to

$$\tilde{R}_{\eta\eta} = C_\eta^0 |\lambda_{\eta\alpha}|^4 \tilde{R}_\alpha^0(r_s), \quad (3.31)$$

where the amplitude of the oscillatory part at half-filling is given by $C_\eta^0 = \tilde{R}_{\eta\alpha}^{cm}(\infty_c)$. The remaining correlation function is independent of the orbital η and given by $\tilde{R}_\alpha^0 = (2\pi a)^{-2}(a/r_s)$.

The large distance limit of the corresponding expression for small doping ($\gamma = \delta$) and low temperature, where $l_\beta \gg r_c \gg l_\delta \gg l_{m_c}$, looks like

$$\tilde{R}_{\eta\eta}^\delta = C_\eta^\delta |\lambda_{\eta\alpha}|^4 \tilde{R}_\alpha^\delta(r_c, r_s). \quad (3.32)$$

In the doped regime, C_η^δ is the amplitude $\tilde{R}_{\eta\alpha}^{cm}(l_\delta)$ obtained in the massive phase at the crossover, as shown in Fig. 4. Like before, the remaining correlation function $\tilde{R}_\alpha^\delta = (2\pi a)^{-2}(a/r_s)(a/r_c)^{K_c^*}$ is also independent of η but shows dependence on spin and charge degrees of freedom. For larger doping rates ($l_\delta < l_{m_c}$), the difference between copper and oxygen sites vanishes.

5. Knight shifts and relaxation rates

The standard expressions for the Knight shifts and for the relaxation rates resulting from a hyperfine coupling term like (2.7) are

$$K_\eta^\gamma = \frac{C_\eta}{\gamma_\eta \gamma_e \hbar^2} \sum_{\eta' = a, b} \chi_{\eta\eta'}^\gamma(\omega = 0, p \rightarrow 0) \quad (3.33)$$

$$\frac{1}{T_{1\eta}^\gamma} = \frac{C_\eta^2}{\gamma_\eta \gamma_e \hbar^2 \beta} \sum_p \frac{\text{Im}[\chi_{\eta\eta}^\gamma(\omega_\eta, p)]}{\omega_\eta}, \quad (3.34)$$

where $\gamma = 0$ refers to the half-filled case and $\gamma = \delta$ to the doped case. ω_η denotes the electronic Zeeman frequency in orbital η , which is very small as compared to the energy scale of the purely electronic system fixed by the cutoff λ . For the Knight shifts the sum is restricted to the active orbitals a and b . We can split up the susceptibility $\chi_{\eta\eta'}^\gamma$ into the non-oscillatory $\bar{\chi}_{\eta\eta'}^\gamma$ and the oscillatory contribution $\tilde{\chi}_{\eta\eta'}^\gamma$ just like for the correlation functions in (3.23). Finally, the Knight shifts for the linearized four-band model in units of $C_\eta/(\gamma_\eta \gamma_e \hbar^2)$ are given by

$$K_\eta^\gamma = \bar{F}_{\eta\alpha} \bar{\chi}_\alpha(\omega = 0, q \rightarrow 0) \quad (3.35)$$

and the relaxation rates in units of $C_\eta^2/(\gamma_\eta \gamma_e \hbar^2 \omega_\eta)$ by

$$\frac{1}{T_{1\eta}^\gamma} = \frac{1}{\beta} \sum_{|q| < \lambda} \text{Im} \left[(\bar{F}_{\eta\alpha})^2 \bar{\chi}_\alpha(\omega_\eta, q) + (\tilde{F}_{\eta\alpha}^\gamma)^2 \tilde{\chi}_\alpha^\gamma(\omega_\eta, q) \right]. \quad (3.36)$$

The susceptibilities $\bar{\chi}_\alpha$ and $\tilde{\chi}_\alpha^\gamma$ in space-time can be obtained from

$$\bar{\chi}_\alpha(x, t) = 2\theta(t) \text{Im}[\bar{R}_\alpha(x, \tau, \beta)]_{\tau=it+\epsilon} \quad (3.37)$$

$$\tilde{\chi}_\alpha^\gamma(x, t) = 2\theta(t) \text{Im}[\tilde{R}_\alpha^\gamma(x, \tau, \beta)]_{\tau=it+\epsilon} \quad (3.38)$$

performing the continuation to real time. The τ -ordered temperature dependent Green's functions on the right-hand side are the same as in (3.24), (3.31) and (3.32), using (3.30). Thus, in general we can calculate (3.35) and (3.36) by performing the Fourier transform of (3.37) and (3.38). Here we restrict ourselves to the solutions obtained by the so called power counting method. The temperature dependences of the Knight shifts and of the relaxation rates are shown in Table I and the form factors $\bar{F}_{\eta\alpha}$ and $\tilde{F}_{\eta\alpha}^\gamma$ are given in Table II.

B. NMR properties of the Bulut model

In order to obtain the NMR properties of the 1D version of the Bulut model we perform the same procedure as before for the four-band model. The bosonized version of the Bulut model (2.28) is given by (3.13) replacing H_N by

$$H_N^{Bu} = \int dx [C_A \mathbf{I}(x) \mathbf{S}_A^{Bu}(x) + C_B \mathbf{J}(x) \mathbf{S}_B^{Bu}(x)] , \quad (3.39)$$

where \mathbf{S}_η^{Bu} is the projection onto the α -band using (2.29), (2.30), (2.8) and (3.4). For the z-component of the spin \mathbf{S}_η^{Bu} we get

$$\begin{aligned} S_A^{zBu}(x) &= 2|\lambda_{Aa}^{Bu}|^2 |\lambda_{a\alpha}|^2 [\bar{s}_\alpha(x) + \cos(2k_F a) \tilde{s}_{a\alpha}(x)] \\ S_B^{zBu}(x) &= 2|\lambda_{Ba}^{Bu}|^2 |\lambda_{a\alpha}|^2 [\bar{s}_\alpha(x) + \cos(k_F a) \tilde{s}_{a\alpha}(x)] \end{aligned} \quad (3.40)$$

ignoring all gradient terms of the field ϕ_c . The spin operators \bar{s}_α and $\tilde{s}_{\eta\alpha}$ are defined as before in (3.19) and (3.20). The NMR properties for a hyperfine coupling like (3.39) are given by (3.35) and (3.36) by the replacements $\bar{F}_{\eta\alpha} \rightarrow \bar{F}_{\eta\alpha}^{Bu}$ and $\tilde{F}_{\eta\alpha} \rightarrow \tilde{F}_{\eta\alpha}^{Bu}$. The values for the different form factors are shown in Table III. At this level of approximation, both the four-band and the Bulut model show exactly the same temperature dependence for the Knight shifts as well as for the relaxation rates; this dependence is different for the uniform contribution and for the oscillatory one (see Table I), as is well known for interacting one-dimensional systems. This effect has nothing to do with the various orbitals where the Knight shifts and the relaxation rates are measured.

C. Comparing the four-band model and the 1D Bulut model

First we focus on the coefficients of the Bulut and of the four-band model (compare Table II and III) related to the different projection procedures of the s-orbitals onto the ground state. For comparing both models, we investigate the limit $t_{ab} \ll (\epsilon_b - \epsilon_a)$. Then, for the four-band model the projection of the s orbitals (A, B) onto the lowest band (α) is strictly done in k -space and results in

$$|\lambda_{B\alpha}(k_F)|^2 \rightarrow 2(\lambda_{Ba}^{Sh})^2 \quad (3.41)$$

$$- 2 \cos(k_F a) (\lambda_{Ba}^{Sh})^2 \quad (3.42)$$

$$|\lambda_{A\alpha}(k_F)|^2 \rightarrow 2(\lambda_{Aa}^{Sh} + \lambda_{Aa}^{Mi})^2 \quad (3.43)$$

$$+ 4(\lambda_{Aa}^{Mi})^2 \quad (3.44)$$

$$+ 2 \cos(2k_F a) (\lambda_{Aa}^{Sh} + \lambda_{Aa}^{Mi})^2 \quad (3.45)$$

$$+ 8 \cos(k_F a) (\lambda_{Aa}^{Sh} + \lambda_{Aa}^{Mi}) \lambda_{Aa}^{Mi} , \quad (3.46)$$

whereas for the Bulut model it is a combination of real space and k -space projection yielding

$$2|\lambda_{Ba}^{Bu}|^2 |\lambda_{a\alpha}(k_F)|^2 \rightarrow 2(\lambda_{Ba}^{Sh})^2 \quad (3.47)$$

$$2|\lambda_{Aa}^{Bu}|^2 |\lambda_{a\alpha}(k_F)|^2 \rightarrow 2(\lambda_{Aa}^{Sh} + \lambda_{Aa}^{Mi})^2 . \quad (3.48)$$

The general solution for the projected O-3s orbital includes one more term (3.42) than the solution proposed

by Bulut (3.47). This term corresponds to a dynamic contribution which includes a charge displacement. However, for a half-filled system the additional term vanishes and the two solutions become identical. By contrast, the projection procedure for the Cu-4s orbital produces a completely different behavior in the two models. For a half-filled system, the hopping processes via $\lambda_{Aa}^{Bu} = \lambda_{Aa}^{Sh} + \lambda_{Aa}^{Mi}$ contribute only in the Bulut model (3.48), whereas they are exactly canceled by the related dynamic terms (3.45) in the four-band model. Thus, for the four-band model at half-filling, only an additional local term (3.44) as well as a dynamic combined term (3.46) remain. The term (3.44) is the local analog to the transferred terms proposed by Mila-Rice, and the term (3.46) is a combination of Mila-Rice and Shastry terms which includes a charge displacement. It should be clear that our projection procedure is the right one for a system with small Coulomb interactions: First we diagonalize the tight-binding Hamiltonian dealing with extended wave functions, and then we treat the Coulomb energy approximately within this non-local basis. The approximation proposed by Bulut suffers from a mismatch between the local and the non-local point of view.

The second part of the oscillatory contribution to the form factors (compare Table II and III), which contains the dependence on the characteristic lengths related to the doping rate, l_δ , as well as to the charge mass, l_{m_c} , is the crucial one. Away from half-filling, the four-band model shows a different behavior on the copper and on the oxygen, despite the fact that umklapp processes only contribute on short or intermediate scales. Indeed, the different hyperbolic dependencies of the two characteristic lengths l_{m_c} and l_δ for copper and for oxygen (see Table II) affect measured quantities related to long distance or long time behavior. Instead, for the Bulut model the difference between copper and oxygen comes in only because of the special choice of a Mila-Rice-Shastry type electron-nuclear interaction term (3.39) and the related unconventional projection procedure which results in the different trigonometric form factors (see Table III). The influence of the charge mass m_c is the same for copper and for oxygen, a fact which manifests itself by the same dependence on the characteristic length l_{m_c} .

Note that the four-band model leads to a very small contribution on the oxygen even at finite doping, because the contribution is exponentially suppressed in a way which depends on the ratio between l_{m_c} and l_δ , whereas the oscillatory contribution on the copper atom is nearly independent of the doping rate for long distances or times. For the ratio between copper and oxygen we distinguish between two regimes:

$$\tanh \left[K_c K_0 \left(\frac{l_\delta}{l_{m_c}} \right) \right] \rightarrow \begin{cases} 1 & \text{for } l_\delta \ll l_{m_c} \\ 0 & \text{for } l_\delta \gg l_{m_c} \end{cases} . \quad (3.49)$$

In the former regime, we recover the Luttinger Liquid behavior, since the infinite length l_{m_c} stems from the vanishing of the umklapp process when $U_{a\alpha} = U_{b\alpha}$; in

that case there is no fundamental difference between copper and oxygen anymore. Only the overlaps with the ground state remain different. The latter regime, where the fundamental difference occurs, will be reached exponentially as $K_c \sqrt{\pi l_{m_c}/2l_\delta} \exp(-l_\delta/l_{m_c})$, and thus the oxygen does not see the antiferromagnetic fluctuations in this limit. Instead, for the Bulut model everything depends on the same correlation function, and the difference between copper and oxygen comes from the filtering factors. Thus, the oscillating contributions to the relaxation rates for the oxygen is always proportional to $[0 + (\pi a/2l_\delta)^2]$, whereas the contributions on copper are reduced by a factor $[1 - (\pi a/l_\delta)^2]$. The ratio of the oscillating contribution to the relaxation rates is approximately given by $(\pi a/2l_\delta)^2$, and is completely independent of the details of the projected local Coulomb repulsions $U_{a\alpha}$ and $U_{b\alpha}$. It only depends on the doping rate and is proportional to $(\delta a/4)^2$. By contrast, the four-band model includes the effect of the Coulomb interactions through its dependence on l_{m_c} . In Table IV we show the ratios of the different Knight shifts and relaxation rates contributions.

IV. THE STRONG INTERACTION LIMIT

For strong interactions the four-band system in (2.1) is much more difficult to solve. Yet, it is still possible to highlight the qualitative features of the transferred hyperfine coupling interaction, specifically for the half-filled case. To obtain the strong interaction limit of this model we can perform the Gutzwiller projection

$$H = \hat{P}(H_0 + H_S + H_N)\hat{P} \quad (4.1)$$

which eliminates doubly occupied states in the Cu-3d orbitals from the Fock space. The projection is effectively performed on all three terms of (4.1), which are treated on equal footing. As far as the first part $\hat{P}H_0\hat{P}$ is concerned, two possible superexchange processes are generated, as shown in Fig. 5. In the strong interaction limit ($U_a \gg |\epsilon_\eta - \epsilon_{\eta'}|, U_b \gg t_{\eta\eta'}$) the superexchange process in Fig. 5(a) is much more effective than the process in Fig. 5(b). For the basic system H_0 , we only have to keep 3 states per unit cell, whereas for the four-band model (4.1), we end up with a system where we have to keep 27 spin-degenerate local states per unit cell j with 4 tight-binding parameters $t_{\eta\eta'}$ for a half-filled system (excluding doubly excited A, B -states, see Appendix C). For a doped system the number of states as well as the number of possible transitions increases very fast, as has been shown for a two-band model.²³ A correct projection procedure such as (4.1) becomes very difficult to handle, and one must resort to some approximations. In any event, in the vicinity of the half-filled case where the projection can be explicitly used for the full Hamiltonian, we will analyze the differences between the predictions of the

four-band model and those of the approximated Hamiltonians. So let us restrict our analysis to the half-filled case where only virtual double occupancies of the copper site are allowed and where electron-nuclear interaction processes require that the initial and the final charge distribution be the same. We deal with electron-nuclear interaction processes where effectively one local Cu-3d spin will be reversed and then relaxed by the thermodynamic fluctuations of the Heisenberg model. We decompose $(H_0 + H_S + H_N)$ into $(L + K)$. L includes all local and K all kinetic contributions of the complete Hamiltonian H introduced in (2.1). Then we can expand $\hat{P}H\hat{P}$ on the basis of the unperturbed eigenstates of L and compute the projected local s-orbital spin operators like $\hat{P}\mathbf{S}\eta j\hat{P}$. For the details we refer to Appendix C and discuss only the final results.

First we analyze some relaxation processes for the oxygen atom. The process shown in Fig. 6(a) is a transferred (T) contribution proportional to

$$F_{B,T,(a)} = \left[\frac{t_{Ba}}{\epsilon_B - (\epsilon_a + U_a)} \right]^2. \quad (4.2)$$

For the process shown in Fig. 6(b), we include a part of the superexchange process to avoid double occupation of the copper site, and the contribution is proportional to

$$F_{B,T,(b)} = \left[\frac{t_{ab}t_{Ba}}{(\epsilon_a - \epsilon_b)(\epsilon_B - \epsilon_b)} \right]^2. \quad (4.3)$$

Then the lowest order contribution to the general form factor for the oxygen is given by

$$F_B(p) = 2F_{B,L} + 2F_{B,T} \cos(pa/2) \quad (4.4)$$

with

$$F_{B,L} = 0 \quad (4.5)$$

$$F_{B,T} = \underbrace{n_{B,T,(a)} F_{B,T,(a)}}_{\text{projected Shastry}} + n_{B,T,(b)} F_{B,T,(b)} + \dots. \quad (4.6)$$

$n_{B,T,(i)}$ denotes the combinatorial factor associated with all possible processes yielding a contribution $F_{B,T,(i)}$. The factor 2 for the left-right symmetry is not included in $n_{B,T,(i)}$. Like for the superexchange processes (Fig. 5) some processes are forbidden due to the Pauli principle. However, since all energy levels are assumed to be spin-independent the related amplitudes $F_{B,T,(i)}$ are the same.

For copper we also distinguish between the transferred (Fig. 7) and the local contributions (Fig. 8). The transferred contributions are proportional to

$$F_{A,T,(a)} = \left[\frac{t_{Ab}t_{ab}}{(\epsilon_A - \epsilon_b)(\epsilon_A + \epsilon_a - 2\epsilon_b - U_b)} \right]^2 \quad (4.7)$$

$$F_{A,T,(b)} = \left[\frac{t_{Ab}t_{ab}}{(\epsilon_A - \epsilon_b)(\epsilon_A - \epsilon_a - U_a)} \right]^2 \quad (4.8)$$

$$F_{A,T,(c)} = \left[\frac{t_{Aa}}{\epsilon_A - \epsilon_a - U_a} \right]^2 \quad (4.9)$$

$$F_{A,T,(d)} = \frac{t_{Ab}t_{ab}t_{Aa}}{(\epsilon_A - \epsilon_b)^2(\epsilon_a - \epsilon_b)}, \quad (4.10)$$

whereas the local contributions are given by

$$F_{A,L,(a)} = \left[\frac{t_{Ab}t_{ab}}{(\epsilon_A - \epsilon_b)(\epsilon_A + \epsilon_a - 2\epsilon_b - U_b)} \right]^2 \quad (4.11)$$

$$F_{A,L,(b)} = \left[\frac{t_{Ab}t_{ab}}{(\epsilon_A - \epsilon_b)(\epsilon_A - \epsilon_a - U_a)} \right]^2 \quad (4.12)$$

$$F_{A,L,(c)} = \left[\frac{t_{Ab}t_{ab}}{(\epsilon_A - \epsilon_b)(\epsilon_A + \epsilon_a - 2\epsilon_b)} \right]^2. \quad (4.13)$$

Then, the general form factor for copper reads

$$F_A(p) = 2F_{A,L} + 2F_{A,T} \cos(pa) \quad (4.14)$$

with

$$F_{A,L} = n_{A,L,(a)}F_{A,L,(a)} + n_{A,L,(b)}F_{A,L,(b)} + n_{A,L,(c)}F_{A,L,(c)} + \dots \quad (4.15)$$

$$F_{A,T} = \underbrace{n_{A,T,(a)}F_{A,T,(a)} + n_{A,T,(b)}F_{A,T,(b)}}_{\text{projected Mila-Rice}} + \underbrace{n_{A,T,(c)}F_{A,T,(c)}}_{\text{projected Shastry}} + n_{A,T,(d)}F_{A,T,(d)} + \dots. \quad (4.16)$$

Let us now compare the predictions of the four-band model and those of the 1D Mila-Rice or Shastry models.

Using the projected expression for the oxygen instead of the unprojected one (2.24), only process (b) in (4.6) contributes in the strong interaction limit, whereas process (a) in (4.6) proposed by Shastry becomes negligible

$$F_{B,T,(a)} \xrightarrow{U_a \rightarrow \infty} 0. \quad (4.17)$$

The form factor for the characteristic wave vectors ($p = 0$ or $p = \pi/a$) is then reduced to

$$F_B(0) = 2n_{B,T,(b)}F_{B,T,(b)} \quad (4.18)$$

$$F_B(\pi/a) = 0. \quad (4.19)$$

Since only the relaxation process of the oxygen nuclear spin contributes, which corresponds to $p \sim 0$, we recover the basic structure of the form factor of Shastry with modified amplitudes. Thus at half-filling, there is no fundamental difference for the oxygen between the general form factor (4.4) and the form factor proposed by Shastry (2.27).

In the strong coupling limit at half filling, the following contributions to the form factor for copper are suppressed:

$$F_{A,L,(b)}, F_{A,T,(b)}, F_{A,T,(c)} \xrightarrow{U_a \rightarrow \infty} 0. \quad (4.20)$$

Thus the projected Shastry contribution (c) in (4.16) and one of the projected Mila-Rice contributions (b) in (4.16) as well as one of the projected local contributions (b) in (4.15) become negligible, and we end up with

$$F_{A,L} = n_{A,L,(a)}F_{A,L,(a)} + n_{A,L,(c)}F_{A,L,(c)} + \dots \quad (4.21)$$

$$F_{A,T} = n_{A,T,(a)}F_{A,T,(a)} + n_{A,T,(d)}F_{A,T,(d)} + \dots \quad (4.22)$$

for the local and for the transferred contributions to the general form factor (4.14), respectively. Thus the uniform part of the form factor is given by

$$F_A(0) = 4n_{A,(a)}F_{A,(a)} + 2n_{A,L,(c)}F_{A,L,(c)} + 2n_{A,T(d)}F_{A,T(d)} + \dots, \quad (4.23)$$

whereas the oscillating part reads

$$F_A(\pi/a) = 2n_{A,L,(c)}F_{A,L,(c)} - 2n_{A,T,(d)}F_{A,T,(d)} + \dots. \quad (4.24)$$

We used the fact that $n_{A,L,(a)} = n_{A,T,(a)} \equiv n_{A,(a)}$ and $F_{A,L,(a)} = F_{A,T,(a)} \equiv F_{A,(a)}$. The uniform part includes contributions which are absent in the 1D version of the Mila-Rice and of the Shastry model. Furthermore, some terms proposed by Shastry turn out to be zero in the strongly interacting limit. For the oscillatory part the effects are much more drastic. The transferred terms proposed by Shastry vanish in the strong coupling regime, whereas other transferred terms, which come from a combination of Mila-Rice and Shastry processes, contribute. Besides, the transferred terms proposed by Mila and Rice are canceled by the equivalent local terms. Hence, in 1D, the general form factor differs both qualitatively and quantitatively from the form factors one would derive from the Mila-Rice or from the Shastry models.

V. DISCUSSION AND PERSPECTIVES

In this paper, we have analyzed the 1D analogs of the hyperfine form factors proposed for NMR measurements of high- T_c materials in the antiferromagnetic phase. We have focused on the situation where one deals with an antiferromagnet generated by a superexchange process via an oxygen atom located at the midpoint between two copper atoms and where the Fermi contact interaction is one of the main contributions to the possible electron-nuclear interaction terms. We have investigated a 1D Cu-O model including four orbitals per unit cell, namely the Cu-3d and the O-2p orbitals governing the ground state properties, as well as the Cu-4s and O-3s orbitals describing the isotropic Fermi contact interaction. In 1D, we were able to solve this model using only standard techniques without having to introduce any additional approximations for the hyperfine interaction term as proposed by Mila-Rice and by Shastry. Thus, we were able to compare our solutions of the four-band model with the predictions of the approximative models.

In the low interaction limit, we have calculated the resulting temperature dependence of the Knight shifts K and of the relaxation rates $1/T_1$ for an undoped and for a doped system; in that limit the ground state is well

described by the strongly hybridized Cu-3d–O-2p anti-bonding band the width of which is large as compared to all Coulomb interactions. For both models, the four-band and the approximative one (Bulut model), the temperature dependences are the same and show the typical power law behavior of one-dimensional interacting systems (see Table I). Within this scope we have shown for the four-band model that for an undoped and a slightly doped system copper and oxygen behave completely different for long distances or long times, when the temperature is low enough. The oxygen nuclei see only the Korringa-like contributions, since the antiferromagnetic contributions are exponentially suppressed depending on the ratio of the characteristic length related to the charge gap and the doping. In contrast, the copper nuclei always see both contributions, the Korringa-like contribution as well as the antiferromagnetic one. This fundamental difference between copper and oxygen vanishes gradually when the characteristic doping length or the characteristic thermal length becomes shorter than the length related to the charge gap (the difference goes away abruptly when the system develops a gap in the spin sector). This solution is at variance with the prediction of the related approximate model, where for oxygen the antiferromagnetic contributions to $1/T_1$ increase with doping like δ^2 , whereas for copper they decrease proportionally to δ^2 . Thus, the scenario where oxygen does not see the antiferromagnetic fluctuations is realized much more effectively in the four-band model than in the 1D version of the models proposed for the high- T_c materials. In 1D, such an unconventional scenario works, since even small interactions generate strong antiferromagnetic correlations due to the drastic reduction of the Fermi surface.

We have also considered the strong interaction limit. Performing a Gutzwiller projection onto the four-band model without further approximations for the electron-nuclear interaction term, we computed the various processes contributing to NMR. Our analysis was limited to the insulating phase (Heisenberg model), since even in 1D a full solution of the model for a doped system (t-J model with four orbitals per unit cell) is unavailable. In the strong interaction limit of the 1D Cu-O model, we were able to compare the form factors obtained for the four-band model with the predictions obtained for the approximate models (Mila-Rice model and Shastry model) investigating the different relaxation processes for the copper and oxygen nuclear spins. In this context, we have shown that neither the 1D analog of the Mila-Rice model nor the 1D analog of the Shastry model could describe the strong interaction limit at half-filling. In contrast to the usual assumption that only transferred contributions are relevant, we predict that both local and transferred contributions should be taken into account for describing the relaxation of the nuclear copper spin via an Cu-4s orbital. Furthermore, we have shown that for infinite local repulsions on the copper sites and small local repulsions on the oxygen sites, the contributions proposed by Mila-Rice and Shastry vanish. For the relax-

ation of the nuclear oxygen spin we recover the basic idea of transferred hyperfine couplings with slightly modified amplitudes, but once again the contribution proposed by Shastry vanishes for infinite repulsion on the copper site.

Both the strong and the weak coupling limits underscore the importance of keeping the full four-band model, at least in one dimension, in order to give an accurate description of the NMR properties. The method we used in the present paper to tackle such a model can thus be extended in various directions. First, it can be applied to study specific models which have a structure similar to the model Cu-O chain analyzed here. This is for example the case for ladder materials such as $\text{Sr}_{14-x}\text{Ca}_x\text{Cu}_{24}\text{O}_{41}$. Analyses of the NMR material have so far been performed in terms of Mila-Rice-Shastry approximations. An analysis retaining the full four-band model, with the specific symmetries of these ladder systems, is currently in progress.²⁴ Other systems for which our analysis can be relevant are TMTSF and TMTTF alloys.⁹ At stoichiometric composition they form an alternate stack.²⁵ Let us now comment on anisotropic contributions to K and to $1/T_1$; these can be produced by a dipolar hyperfine coupling (see Appendix A). They also stem from the specific structural details of a given compound which may lead to an anisotropic form for the susceptibility: in that situation the anisotropy of the $p = 0$ component (3.37) will usually be different from that of the $p = 2k_F$ part (3.38). In both the weak and the strong interaction limits, we find that – for low enough temperature – $1/T_1$ is mostly determined by (3.38), whereas K is proportional to (3.37). The experimental observation that $1/T_1$ is essentially isotropic and that K is anisotropic suggest that anisotropic effects are not too important for the $p = 2k_F$ contributions but do affect the $p = 0$ terms.

Another possible extension of our work concerns of course the two-dimensional systems. Although it is unclear how much of the weak coupling approach remains valid in higher dimension, our strong coupling analysis can straightforwardly be applied to higher dimensional structures. The main difference in that case between the 2D (or higher) and the 1D study presented here comes from the symmetry of the various orbitals. In the case of a Cu-O plane, in the presence of a Coulomb repulsion on the oxygen sites ($U_{\text{O}-2p} \neq 0$),²⁶ the related amplitudes for the local processes (4.11) and (4.13) are not equal anymore, and a cancellation of these terms by symmetry arguments as assumed by Mila-Rice does not occur. Only the contribution like (4.12) will vanish by symmetry arguments. The transferred Mila-Rice contributions (4.7) via the O-2p orbital, which always cost the Coulomb energy $U_{\text{O}-2p}$, and the local processes (4.11) have exactly the same combinatorial factor and the same amplitude; thus the term (4.11) cancels out the term (4.7) for the antiferromagnetic wave vector. This suggests for $U_{\text{Cu}-3d} \rightarrow \infty$ that the antiferromagnetic contribution to the relaxation of the copper nuclei via an isotropic interaction comes from local terms (see (4.13)) and from new transferred combined terms of third order (see (4.10)),

while the transferred contributions proposed up to now are absent (see (4.8) and (4.9)).

ACKNOWLEDGMENTS

This work was initiated by a suggestion from the late H.J. Schulz whom we wish to acknowledge here.

APPENDIX A: ANISOTROPIC HYPERFINE COUPLINGS

Taking into account anisotropic hyperfine couplings related to the orbitals Cu-3d and O-2p we have to replace (2.7) by

$$H'_N = \sum_{j\varsigma} C_A I_j^\varsigma S_{A,j}^\varsigma + C_a I_j^\varsigma S_{a,j}^\varsigma + C_B J_j^\varsigma S_{B,j}^\varsigma + C_b J_j^\varsigma S_{b,j}^\varsigma \quad (\text{A1})$$

The sum on ς is over components of the diagonal hyperfine tensors C_η^ς .

In the weak interaction limit of the four-band model we can perform the same calculations as done before, and we will end up with the bosonized expression (3.13), where now the electron-nuclear interaction is given by

$$H_N = \sum_\varsigma \int dx (C_A |\lambda_{A\alpha}|^2 + C_a^\varsigma |\lambda_{a\alpha}|^2) I^\varsigma (\bar{S}_\alpha^\varsigma + \tilde{S}_{a\alpha}^\varsigma) + \sum_\varsigma \int dx (C_B |\lambda_{B\alpha}|^2 + C_b^\varsigma |\lambda_{b\alpha}|^2) J^\varsigma (\bar{S}_\alpha^\varsigma + \tilde{S}_{b\alpha}^\varsigma) \quad (\text{A2})$$

Here we used the fact that $\tilde{S}_{A\alpha}^\varsigma = \tilde{S}_{a\alpha}^\varsigma$ and $\tilde{S}_{B\alpha}^\varsigma = \tilde{S}_{b\alpha}^\varsigma$. In general the explicit bosonized expressions for the spin part of $\tilde{S}_{\eta\alpha}^x$ and $\tilde{S}_{\eta\alpha}^y$ in (3.20) differ from $\tilde{S}_{\eta\alpha}^z$, but finally for a spin-symmetric model there will be no influence on the correlation functions. Thus only the coefficients are slightly modified and vary for the different directions $\varsigma = x, y, z$. Formally the contributions to the ς -directions of the Knight shifts K_{Cu}^ς and K_{O}^ς , as well as the contributions to the relaxation times $T_{1,Cu}^\varsigma$ and $T_{1,O}^\varsigma$ are given by (3.35) and (3.36) performing the replacements

$$|\lambda_{A\alpha}|^2 \rightarrow |\lambda_{A\alpha}|^2 + \frac{C_a^\varsigma}{C_A} |\lambda_{a\alpha}|^2 \quad (\text{A3})$$

$$|\lambda_{B\alpha}|^2 \rightarrow |\lambda_{B\alpha}|^2 + \frac{C_b^\varsigma}{C_B} |\lambda_{b\alpha}|^2 \quad (\text{A4})$$

in the expressions of the form factors defined in Table II.

In the strong interaction limit of the four-band model the inclusion of anisotropic hyperfine interactions results in

$$\begin{aligned} H''_N = & \sum_{j\varsigma} (2C_A F_{A,L} + C_a^\varsigma F_{a,L}) I_j^\varsigma S_{a,j}^\varsigma \\ & + \sum_{j\varsigma} F_{A,T} I_j^\varsigma (S_{a,j-1}^\varsigma + S_{a,j+1}^\varsigma) \\ & + \sum_{j\varsigma} (C_B F_{B,T} + C_b^\varsigma F_{b,T}) J_j^\varsigma (S_{a,j}^\varsigma + S_{a,j+1}^\varsigma) . \quad (\text{A5}) \end{aligned}$$

Here the new defined parameters which describe the additional couplings to the local Cu-3d spins are given by $F_{a,L} = 1$ and $F_{b,T} = t_{ab}^2/(\epsilon_a - \epsilon_b)^2$, whereas all the others were defined in Section IV. For the copper atom the local contribution is modified, whereas for the oxygen atom it is the transferred one.

APPENDIX B: THE SINE-GORDON MODEL

At half-filling the spin part as well as the charge part of the Hamiltonian (3.13) are described by a sine-Gordon model $H_{SG}^\nu = H_0^\nu + H_U^\nu$ where

$$H_U^\nu = \frac{2aU_\nu}{(2\pi a)^2} \int_0^L dx \cos[\sqrt{8}\Phi_\nu] \quad (\text{B1})$$

For this model two different regimes exist depending on the value of the parameter K_ν . A massive regime (ν_m) for

$$2\pi u_\nu (K_\nu - 1) < |U_\nu| , \quad (\text{B2})$$

where the perturbation of H_U^ν is relevant, and a massless (ν_o) for

$$2\pi u_\nu (K_\nu - 1) > |U_\nu| , \quad (\text{B3})$$

where the perturbation is irrelevant.

1. Massive regime (ν_m)

When the cosine term is relevant, the conformal symmetry is lost and the elementary excitations become massive particles. To compute the correlation functions we can approximate the cosine term by

$$H_m^\nu = \frac{m_\nu^2}{2} \int_0^L dx (\Phi_\nu - \langle \Phi_\nu \rangle)^2 , \quad (\text{B4})$$

where the mass can be obtained from the exact solution of the sine-Gordon equation. For small U_ν one has

$$m_\nu = \left(\frac{4K_\nu |U_\nu| a}{\pi u_\nu} \right)^{\frac{1}{2-2K_\nu}} a^{-1} . \quad (\text{B5})$$

This Hamiltonian describes the fluctuations $\delta\Phi_\nu$ of Φ_ν about its mean value $\langle \Phi_\nu \rangle = 0$. For such a system the Green's function $\langle T_\tau \Phi_\nu(\mathbf{r}_\nu) \Phi_\nu(\mathbf{0}) \rangle_{\nu_m}$ of the Laplace operator defined on the domain $A_\nu = [0 < u_\nu \tau < u_\nu \beta, 0 < x < L]$ is given by

$$G^{\nu_m}(r_\nu) = \frac{K_\nu}{2} K_0[m_\nu(r_\nu + a)] . \quad (\text{B6})$$

K_0 is the Bessel function of zero order.

2. Massless regime (ν_o)

In this regime, the bare parameters are renormalized up to the fixed point values $u_\nu \rightarrow u_\nu^*$, $K_\nu \rightarrow K_\nu^*$, and $U_\nu \rightarrow 0$ without changing the basic Luttinger Liquid behavior of the unperturbed part H_0^ν . For this model, the Green's functions for the unperturbed part regularized for large distances by R_ν and for short distances by the lattice constant a can be expressed as

$$G^{\nu_o}(r_\nu) = \frac{K_\nu}{2} \ln[R_\nu/(r_\nu + a)] \quad (\text{B7})$$

or as the following limit

$$G^{\nu_o}(r_\nu) = \lim_{m_\nu \rightarrow 0} G^{\nu_m}(r_\nu) \quad (\text{B8})$$

3. Correlation functions

Typical spin-spin correlation functions of the original fermions defined in (3.12) are combinations of exponentials of Φ_ν . For a Gaussian model these functions can be expressed in terms of the Green's functions (B6) or (B7) depending on the phase ν_i ,

$$\langle \exp[i\gamma_1 \Phi_\nu(1)] \dots \exp[i\gamma_N \Phi_\nu(N)] \rangle_{\nu_i} = e^{-\sum_{n>m}^N \gamma_n \gamma_m G^{\nu_i}(r_\nu^{nm})} e^{-\frac{1}{2} \sum_n \gamma_n^2 G^{\nu_i}(r_\nu^{nn})} . \quad (\text{B9})$$

APPENDIX C: LOCAL STATES IN THE STRONG INTERACTION LIMIT

The projected Hamiltonian (2.1) is expressed as

$$\hat{P}H\hat{P} = \hat{P}(L + K)\hat{P} , \quad (\text{C1})$$

where L denotes the local system, whereas K includes all possible hopping terms of H . The eigenstates of L are given by

$$|n_1, n_2, \dots, n_j, \dots, n_N\rangle = \prod_{j=1}^N |n_j\rangle , \quad (\text{C2})$$

where n_j labels the local states n on site j . The local states and energies are shown in Table V. For simplicity we use the short notation

$$|0_1, 0_2, \dots, n_j, \dots, m_i, \dots, 0_{N-1}, 0_N\rangle \equiv |n_j, m_i\rangle \quad (\text{C3})$$

(local ground state configurations are labeled by $|0_j\rangle$). The energy of such a state is given by

$$E_{n,m} = (N - 2)\epsilon_0 + \epsilon_n + \epsilon_m . \quad (\text{C4})$$

Now, we can expand the projection operator \hat{P} onto the unperturbed eigenstates of L . Here for the half-filled case, we are only interested in the projection \hat{P} onto the state $|0\rangle = \prod_{j=1}^N |0_j\rangle$ with the energy $E_0 = N\epsilon_0$, thus we get

$$\hat{P} = \sum_i \hat{P}^{(i)} , \quad (\text{C5})$$

where the first orders are given by

$$\begin{aligned} \hat{P}^{(0)} &= \hat{P}_P \\ \hat{P}^{(1)} &= \hat{P}_{PQ} + \hat{P}_{QP} \\ \hat{P}^{(2)} &= \hat{P}_{PQQ} + \hat{P}_{QPP} + \hat{P}_{QQP} \\ &\quad - (\hat{P}_{PPQ^2} + \hat{P}_{PQ^2P} + \hat{P}_{Q^2PP}) \end{aligned} \quad (\text{C6})$$

with

$$\begin{aligned} \hat{P}_P &= \hat{P}_0 \\ \hat{P}_{PQ} &= \hat{P}_0 K \hat{Q}_0 \frac{1}{E_0 - L} \hat{Q}_0 \\ \hat{P}_{QP} &= \hat{Q}_0 \frac{1}{E_0 - L} \hat{Q}_0 K \hat{P}_0 \\ \hat{P}_{PQQ} &= \hat{P}_0 K \hat{Q}_0 \frac{1}{E_0 - L} \hat{Q}_0 K \hat{Q}_0 \frac{1}{E_0 - L} \hat{Q}_0 \\ \hat{P}_{QPP} &= \hat{Q}_0 \frac{1}{E_0 - L} \hat{Q}_0 K \hat{P}_0 K \hat{Q}_0 \frac{1}{E_0 - L} \hat{Q}_0 \\ \hat{P}_{QQP} &= \hat{Q}_0 \frac{1}{E_0 - L} \hat{Q}_0 K \hat{Q}_0 \frac{1}{E_0 - L} \hat{Q}_0 K \hat{P}_0 \\ \hat{P}_{PPQ^2} &= \hat{P}_0 K \hat{P}_0 K \hat{Q}_0 \frac{1}{(E_0 - L)^2} \hat{Q}_0 \\ \hat{P}_{PQ^2P} &= \hat{P}_0 K \hat{Q}_0 \frac{1}{(E_0 - L)^2} \hat{Q}_0 K \hat{P}_0 \\ \hat{P}_{Q^2PP} &= \hat{Q}_0 \frac{1}{(E_0 - L)^2} \hat{Q}_0 K \hat{P}_0 K \hat{P}_0 \end{aligned} \quad (\text{C7})$$

The projection operator \hat{Q}_0 denotes $1 - \hat{P}_0$.

We can compute the projected electron-nuclear interaction term $\hat{P}H_N\hat{P}$. The projection affects only the electronic spins, and we have to evaluate projected local s orbital spin operators such as $\hat{P}\mathbf{S}_{\eta j}\hat{P}$. For example, the second order processes (see Fig. 6(a) and 7(c)) are given by

$$\mathbf{S}_{\eta j}^{(2)} = (\hat{P}^{(0)} + \hat{P}^{(1)}) \mathbf{S}_{A j} (\hat{P}^{(0)} + \hat{P}^{(1)}) \quad (\text{C8})$$

Introducing (C6) and (C7) in (C8) only

$$\mathbf{S}_{A j}^{(2)} = \hat{P}_{PQ} \mathbf{S}_{A j} \hat{P}_{QP} \quad (\text{C9})$$

will contribute, because in a half-filled system the first hopping process brings the system out of the ground state

$|0\rangle$ and the second one brings it back to a possible ground state configuration $|0\rangle$. Here only the projections

$$\hat{P}_{PQ} = \frac{t_{Aa}}{E_0 - E_{\bar{4},13}} |0\rangle \langle \bar{4}_j, 13_{j\pm 1}| \quad (\text{C10})$$

$$\hat{P}_{QP} = \frac{t_{Aa}}{E_0 - E_{\bar{4},13}} |\bar{4}_j, 13_{j\pm 1}\rangle \langle 0| \quad (\text{C11})$$

could generate finite matrix elements for second order contributions to the Cu-4s spin \mathbf{S}_{A_j} . For the O-3s spin \mathbf{S}_{B_j} it will be

$$\hat{P}_{PQ} = \frac{-t_{Ba}}{E_0 - E_{12}} |0\rangle \langle 12_j| \quad (\text{C12})$$

$$\hat{P}_{QP} = \frac{-t_{Ba}}{E_0 - E_{12}} |12_j\rangle \langle 0| \quad (\text{C13})$$

or

$$\hat{P}_{PQ} = \frac{t_{Ba}}{E_0 - E_{\bar{2},13}} |0\rangle \langle \bar{2}_j, 13_{j+1}| \quad (\text{C14})$$

$$\hat{P}_{QP} = \frac{t_{Ba}}{E_0 - E_{\bar{2},13}} |\bar{2}_j, 13_{j+1}\rangle \langle 0| . \quad (\text{C15})$$

Finally, the projected spins $\mathbf{S}_{\eta j}^{(2)}$ are given by

$$\mathbf{S}_{A_j}^{(2)} = |\lambda_{Aa}|^2 \hat{P}_0 (\mathbf{S}_{a,j-1} + \mathbf{S}_{a,j+1}) \hat{P}_0 \quad (\text{C16})$$

$$\mathbf{S}_{B_j}^{(2)} = |\lambda_{Ba}|^2 \hat{P}_0 (\mathbf{S}_{a,j} + \mathbf{S}_{a,j+1}) \hat{P}_0 . \quad (\text{C17})$$

with

$$\lambda_{Aa} = \frac{t_{Aa}}{\epsilon_A - \epsilon_a - U_a} \quad (\text{C18})$$

$$\lambda_{Ba} = \pm \frac{t_{Ba}}{\epsilon_B - \epsilon_a - U_a} . \quad (\text{C19})$$

Higher order contributions could be computed using the same procedure as for the above examples.

¹¹ We wish to thank D. Jerome and P. Wzietek for helpful discussions on this issue.

¹² E. B. Stechel, A. Sudbø, T. Giamarchi, and C. M. Varma, Phys. Rev. B **51**, 553 (1995).

¹³ F. C. Zhang and T. M. Rice, Phys. Rev. B **37**, 3759 (1988).

¹⁴ D. C. Mattis, J. Math. Phys. **15**, 609 (1974).

¹⁵ A. Luther and I. Peschel, Phys. Rev. B **9**, 2911 (1974).

¹⁶ F. D. M. Haldane, J. Phys. C **14**, 2585 (1981).

¹⁷ R. Heidenreich, R. Seiler, and D. A. Uhlenbrock, J. Stat. Phys. **22**, 27 (1980).

¹⁸ F. D. M. Haldane, Phys. Rev. Lett. **45**, 1358 (1980).

¹⁹ H. J. Schulz, Phys. Rev. Lett. **64**, 2831 (1990).

²⁰ A. Sudbø *et al.*, Phys. Rev. Lett. **70**, 978 (1993).

²¹ T. Giamarchi and H. J. Schulz, Phys. Rev. B **39**, 4620 (1989).

²² A. M. Tsvelik, *Quantum Field Theory in Condensed Matter Physics* (Cambridge University Press, Cambridge, 1995).

²³ J. Zaanen and A. Oleś, Phys. Rev. B **37**, 9423 (1988).

²⁴ T. Becker, M. Gabay, and T. Giamarchi, to be published.

²⁵ V. Ilakovac *et al.*, Phys. Rev. B **50**, 7136 (1994).

²⁶ T. Becker, M. Gabay, and T. Giamarchi, to be published.

¹ A. J. Millis, H. Monien, and D. Pines, Phys. Rev. B **42**, 167 (1990).

² F. Mila and T. M. Rice, Physica C **157**, 561 (1989).

³ B. S. Shastry, Phys. Rev. Lett. **63**, 1288 (1989).

⁴ P. W. Anderson, Adv. Phys. **46**, 3 (1997).

⁵ Y. Zha, V. Barzykin, and D. Pines, Phys. Rev. B **54**, 7561 (1996).

⁶ A. J. Millis and H. Monien, Phys. Rev. B **45**, 3059 (1992).

⁷ N. Bulut, D. W. Hone, D. J. Scalapino, and N. E. Bickers, Phys. Rev. B **41**, 1797 (1990).

⁸ C. M. Varma, Phys. Rev. Lett. **77**, 3431 (1996).

⁹ D. Jérôme and H. J. Schulz, Adv. Phys. **31**, 299 (1982).

¹⁰ C. Bourbonnais and D. Jerome, in *Advances in Synthetic Metals, Twenty years of Progress in Science and Technology*, edited by P. Bernier, S. Lefrant, and G. Bidan (Elsevier, New York, 1999), pp. 206–301.

TABLE I. The lowest order temperature dependence of the Knight shifts and of the relaxation rates measured on the copper site (A) or the oxygen site (B) at half-filling (0) and for finite doping (δ). Within a line, the undefined constants $const.$ are the same for copper and oxygen. Temperature dependences are given up to logarithmic corrections.

Copper	Oxygen
K_η^0	$\bar{F}_{A\alpha} \times const.$
K_η^δ	$\bar{F}_{A\alpha} \times const.$
$1/\bar{T}_{1\eta}^0$	$(\bar{F}_{A\alpha})^2 \times const. \times T$
$1/\bar{T}_{1\eta}^0$	$(\tilde{F}_{A\alpha}^0)^2 \times const.$
$1/\bar{T}_{1\eta}^\delta$	$(\bar{F}_{A\alpha})^2 \times const. \times T$
$1/\bar{T}_{1\eta}^\delta$	$(\tilde{F}_{A\alpha}^\delta)^2 \times const. \times T^{K_c^*}$
	$(\bar{F}_{B\alpha})^2 \times const. \times T$
	$(\tilde{F}_{B\alpha}^0)^2 \times const.$
	$(\bar{F}_{B\alpha})^2 \times const. \times T$
	$(\tilde{F}_{B\alpha}^\delta)^2 \times const. \times T^{K_c^*}$

TABLE II. $\bar{F}_{\eta\alpha}$ and $\tilde{F}_{\eta\alpha}^\gamma$ are the non-oscillating and the oscillating contributions to the form factors of the four-band model in the weak interaction limit at half-filling ($\gamma = 0$) and for small doping ($\gamma = \delta$) for copper (A) and oxygen (B). The coefficients $\lambda_{\eta\alpha}$ come from the projection onto the lowest band (α) for small Coulomb interaction. l_δ and l_{mc} denote the characteristic lengths related to the doping and the mass for a charge-gap system and K_c is the Luttinger liquid parameter which controls the anomalous exponents of the correlation functions. Finally, K_0 is the Bessel function of zero order.

Copper	Oxygen
$\bar{F}_{\eta\alpha}$	$ \lambda_{A\alpha} ^2$
$(\tilde{F}_{\eta\alpha}^0)^2$	$2 \lambda_{A\alpha} ^4 \left(\frac{a}{l_{mc}}\right)^{K_c}$
$(\tilde{F}_{\eta\alpha}^\delta)^2$	$2 \lambda_{A\alpha} ^4 \cosh \left[K_c K_0 \left(\frac{l_\delta}{l_{mc}} \right) \right] \left(\frac{a}{l_{mc}} \right)^{K_c}$
	$ \lambda_{B\alpha} ^2$
	0
	$2 \lambda_{B\alpha} ^4 \sinh \left[K_c K_0 \left(\frac{l_\delta}{l_{mc}} \right) \right] \left(\frac{a}{l_{mc}} \right)^{K_c}$

TABLE III. The non-oscillating and oscillating form factors at half-filling ($\gamma = 0$) and for small doping ($\gamma = \delta$) for copper and oxygen. $\bar{F}_{\eta\alpha}^{Bu}$ and $\tilde{F}_{\eta\alpha}^{\gamma Bu}$ denote the form factors obtained for the weak interaction Bulut model with a Mila-Rice and Shastry like isotropic electron nuclear interaction term. The coefficients $\lambda_{\eta\alpha}$ are given by (3.4) and (3.5). By contrast, $\lambda_{\eta\alpha}^{Bu}$ is the characteristic coefficient of the Bulut model related to the overlap between the Cu-4s orbitals (A) the Cu-3d orbitals (a) or respectively between the O-3s orbitals (B) and the Cu-3d orbitals (a) performed in real space. The other parameters were explained in Table II.

Copper	Oxygen
$\bar{F}_{\eta\alpha}^{Bu}$	$2 \lambda_{Aa}^{Bu} ^2 \lambda_{a\alpha} ^2$
$(\tilde{F}_{\eta\alpha}^{0Bu})^2$	$8 \lambda_{Aa}^{Bu} ^4 \lambda_{a\alpha} ^4 \left(\frac{a}{l_{mc}}\right)^{K_c}$
$(\tilde{F}_{\eta\alpha}^{\delta Bu})^2$	$8 \lambda_{Aa}^{Bu} ^4 \lambda_{a\alpha} ^4 \cos(\pi a/l_\delta)^2 \cosh \left[K_c K_0 \left(\frac{l_\delta}{l_{mc}} \right) \right] \left(\frac{a}{l_{mc}} \right)^{K_c}$
	$2 \lambda_{Ba}^{Bu} ^2 \lambda_{a\alpha} ^2$
	0
	$8 \lambda_{Ba}^{Bu} ^4 \lambda_{a\alpha} ^4 \sin(\pi a/2l_\delta)^2 \cosh \left[K_c K_0 \left(\frac{l_\delta}{l_{mc}} \right) \right] \left(\frac{a}{l_{mc}} \right)^{K_c}$

TABLE IV. The ratios of the oscillating and non-oscillating contributions to the oxygen ($\eta = B$) and the copper ($\eta = A$) Knight shifts and relaxation rates at half-filling (0) and away from half-filling (δ) calculated for the Bulut and the four-band model in the low interaction limit. The ratios are measured in units of their characteristic overlaps with the ground state ($|\lambda_{\eta a}^{Bu}| |\lambda_{a\alpha}|$ or $|\lambda_{\eta\alpha}|$). Here the oscillating contributions do depend on the characteristic length l_{mc} and l_δ , whereas the non-oscillating contributions do not.

	Bulut model	Four-band model
$\frac{K_B^{0,\delta}}{K_A^{0,\delta}}$	1	1
$\frac{1/\bar{T}_{1B}^{0,\delta}}{1/\bar{T}_{1A}^{0,\delta}}$	1	1
$\frac{1/\tilde{T}_{1B}^0}{1/\tilde{T}_{1A}^0}$	0	0
$\frac{1/\tilde{T}_{1B}^\delta}{1/\tilde{T}_{1A}^\delta}$	$\frac{\sin(\pi a/2l_\delta)^2}{\cos(\pi a/l_\delta)^2}$	$\tanh\left[K_c K_0\left(\frac{l_\delta}{l_{mc}}\right)\right]$

TABLE V. Possible local states per unit cell of the four band Hubbard model. The degeneracy is related to the possible spin configurations for a local state labeled by $|n_j\rangle$.

degeneracy	local energies	state
2	$\epsilon_7 = \epsilon_A + 2\epsilon_B$	$ \bar{7}_j\rangle$
2	$\epsilon_6 = 2\epsilon_A + \epsilon_B$	$ \bar{6}_j\rangle$
1	$\epsilon_5 = 2\epsilon_A + 2\epsilon_B$	$ \bar{5}_j\rangle$
4	$\epsilon_4 = \epsilon_A + 2\epsilon_B + \epsilon_a$	$ \bar{4}_j\rangle$
4	$\epsilon_3 = \epsilon_A + 2\epsilon_B + \epsilon_b$	$ \bar{3}_j\rangle$
4	$\epsilon_2 = 2\epsilon_A + \epsilon_B + \epsilon_a$	$ \bar{2}_j\rangle$
4	$\epsilon_1 = 2\epsilon_A + \epsilon_B + \epsilon_b$	$ \bar{1}_j\rangle$
2	$\epsilon_0 = 2\epsilon_A + 2\epsilon_B + \epsilon_a$	$ 0_j\rangle$
2	$\epsilon_1 = 2\epsilon_A + 2\epsilon_B + \epsilon_b$	$ 1_j\rangle$
8	$\epsilon_2 = \epsilon_A + 2\epsilon_B + \epsilon_a + \epsilon_b$	$ 2_j\rangle$
2	$\epsilon_3 = \epsilon_A + 2\epsilon_B + 2\epsilon_b + U_b$	$ 3_j\rangle$
8	$\epsilon_4 = 2\epsilon_A + \epsilon_B + \epsilon_a + \epsilon_b$	$ 4_j\rangle$
2	$\epsilon_5 = 2\epsilon_A + \epsilon_B + 2\epsilon_b + U_b$	$ 5_j\rangle$
4	$\epsilon_6 = 2\epsilon_A + 2\epsilon_B + \epsilon_a + \epsilon_b$	$ 6_j\rangle$
4	$\epsilon_7 = \epsilon_A + 2\epsilon_B + \epsilon_a + 2\epsilon_b + U_b$	$ 7_j\rangle$
1	$\epsilon_8 = 2\epsilon_A + 2\epsilon_B + 2\epsilon_b + U_b$	$ 8_j\rangle$
4	$\epsilon_9 = 2\epsilon_A + \epsilon_B + \epsilon_a + 2\epsilon_b + U_b$	$ 9_j\rangle$
2	$\epsilon_{10} = 2\epsilon_A + 2\epsilon_B + \epsilon_a + 2\epsilon_b + U_b$	$ 10_j\rangle$
2	$\epsilon_{11} = \epsilon_A + 2\epsilon_B + 2\epsilon_a + U_a$	$ 11_j\rangle$
2	$\epsilon_{12} = 2\epsilon_A + \epsilon_B + 2\epsilon_a + U_a$	$ 12_j\rangle$
1	$\epsilon_{13} = 2\epsilon_A + 2\epsilon_B + 2\epsilon_a + U_a$	$ 13_j\rangle$
4	$\epsilon_{14} = \epsilon_A + 2\epsilon_B + 2\epsilon_a + U_a + \epsilon_b$	$ 14_j\rangle$
4	$\epsilon_{15} = 2\epsilon_A + \epsilon_B + 2\epsilon_a + U_a + \epsilon_b$	$ 15_j\rangle$
2	$\epsilon_{16} = 2\epsilon_A + 2\epsilon_B + 2\epsilon_a + U_a + \epsilon_b$	$ 16_j\rangle$
2	$\epsilon_{17} = \epsilon_A + 2\epsilon_B + 2\epsilon_a + U_a + 2\epsilon_b + U_b$	$ 17_j\rangle$
2	$\epsilon_{18} = 2\epsilon_A + \epsilon_B + 2\epsilon_a + U_a + 2\epsilon_b + U_b$	$ 18_j\rangle$
1	$\epsilon_{19} = 2\epsilon_A + 2\epsilon_B + 2\epsilon_a + U_a + 2\epsilon_b + U_b$	$ 19_j\rangle$

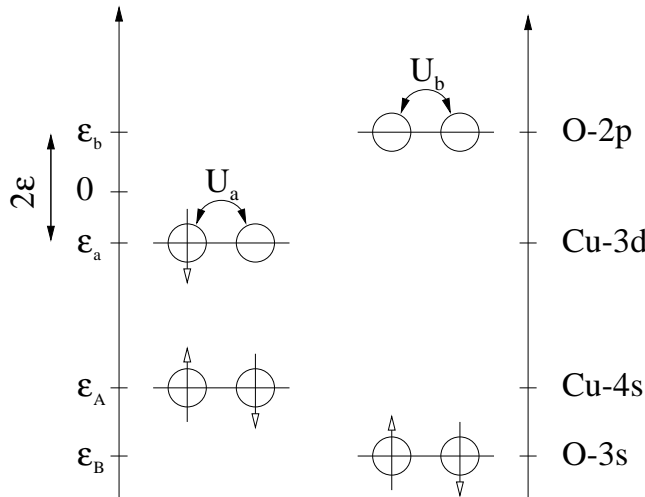


FIG. 1. Energy of the various orbitals. The Cu-3d and O-2p (resp. a and b) orbitals are the relevant ones to describe the electronic degrees of freedom. The Cu-4s and O-3s (resp. A and B) should be kept to describe the coupling to the nuclear spin via a Fermi contact interaction.

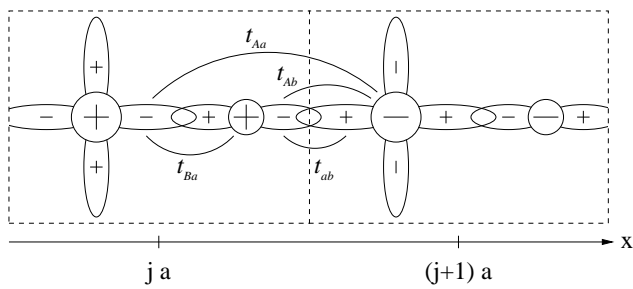


FIG. 2. Cu-3d and Cu-4s orbitals as well as the O-2p and O-3s orbitals in the unit cells. The chosen signs of the wave functions determine the phase convention for the Hamiltonian and the signs of the various tight-binding parameters $t_{\eta\eta'}$.

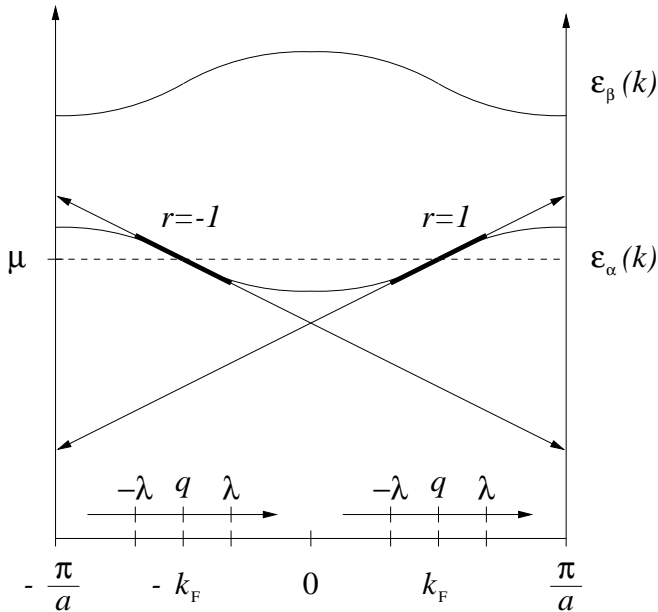


FIG. 3. Linearization of the spectrum close to the Fermi points. The momentum k is replaced by $rk_F + q$, where $r = \pm$ denotes the two possible directions. $\lambda > |q|$ is an ultraviolet cutoff of the order of the bandwidth and the Fermi velocity is $v_F = \partial_k \epsilon_\alpha(k)|_{k_F}$.

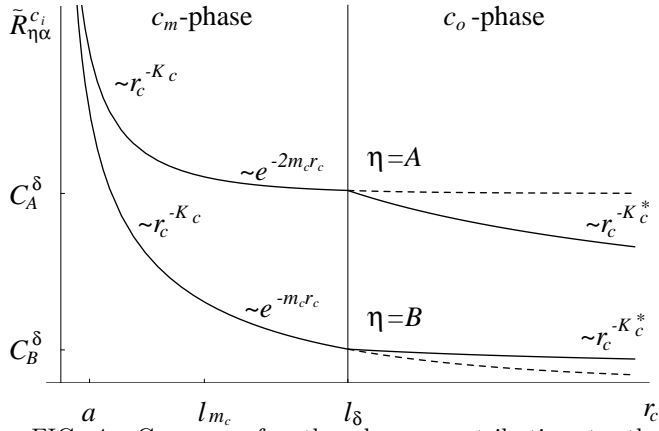


FIG. 4. Crossover for the charge contribution to the spin-spin correlation function $\tilde{R}_{\eta\alpha}^{ci}$ from the massive charge regime (c_m -phase) to the massless charge regime (c_o -phase) at low temperature and for small doping. The behavior for copper (A) and oxygen (B) is quite different: For copper the amplitude remains finite for long distance, whereas the amplitude for oxygen vanishes.

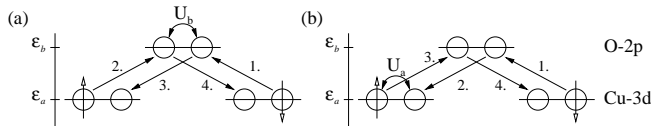


FIG. 5. Superexchange processes generating antiferromagnetic couplings between localized copper spins at half-filling. In contrast to the superexchange path (a) process (b) is suppressed, because it includes an intermediate state where it is necessary to pay the local Coulomb repulsion U_a . The numbers (1.,2.,3., and 4.) denote the sequence of the intermediate steps.

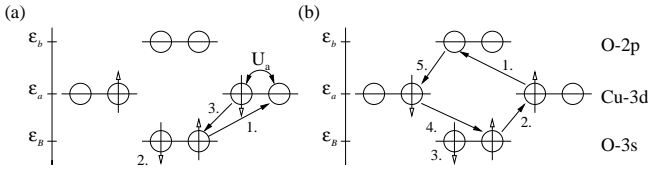


FIG. 6. Possible spin flip processes of the nuclear oxygen spin via a Fermi contact interaction at half-filling. (a) is present in the 1D version of the Shastry model, whereas (b) is another possible process which includes some superexchange contributions. At half-filling there are only transferred contributions (T), local processes (L) are absent. The numbers (1.,2.,3.,4. and 5.) denote the sequence of the intermediate steps.

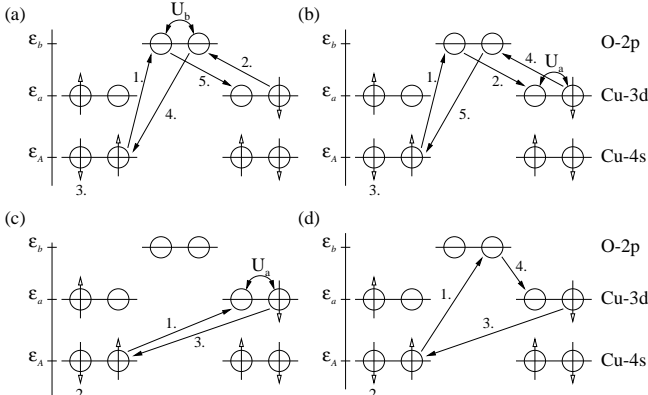


FIG. 7. Possible transferred spin flip processes of the nuclear copper spin like $\hat{P}S_{Aj}^+\hat{P}$ via a Fermi contact interaction at half-filling. (a) and (b) appear in the 1D Mila-Rice model, (c) pertains to the 1D the Shastry model, whereas (d) is a combination of both.

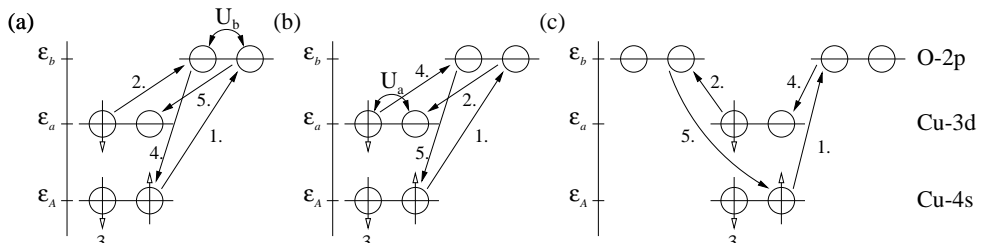


FIG. 8. Possible local spin flip processes of the nuclear copper spin like $\hat{P}S_{Aj}^+\hat{P}$ via a Fermi contact interaction at half-filling. All processes include the O-2p orbital as an intermediate state and are of the same order as the transferred hyperfine coupling processes proposed by Mila and Rice.